Transmission properties at microwave frequencies of two-dimensional metallic lattices

Enrique A. Navarro, Juan Martinez-Pastor,[a] and Vicente Such
Departamento de Física Aplicada, Universitat de València, 46100 Burjassot (València), Spain

(Received 13 January 1999; accepted for publication 19 April 1999)

The transmission properties of different metallic photonic lattices (square and rectangular) have been experimentally studied. A numerical algorithm based on time domain finite differences has been used for simulating these photonic structures. The introduction of defects in the two-dimensional metallic lattice modifies its transmission spectrum. If metal rods are eliminated from (or added to) the lattice, extremely narrow peaks are observed at some particular frequencies below (or above) the band pass edge. © *1999 American Institute of Physics.* [S0021-8979(99)00415-6]

I. INTRODUCTION

Many different photonic crystals have been fabricated so far,[1,2] having spatial periodicity in one, two, or three directions. The main feature of these structures is the existence of frequency regions in which electromagnetic waves cannot propagate: the photonic band gap. Recently, a great interest has been paid to fabricate structures with potential applications as electromagnetic components operating over a wide frequency band. Much of the developed effort has been focused on the use of purely dielectric materials, whereas metallic ones have received little attention due to the consideration of heavy losses in the metal parts. However, metallic photonic structures have some primary advantages over the correspondent with dielectrics: light weight, reduced size, lower cost, and fabrication versatility.[3,4] A more important feature lies in the photonic band gap, which extends from zero frequency up to the first band pass edge, meanwhile pure dielectric photonic structures exhibit a relatively narrow forbidden band gap. On the other hand, the performances of dielectric structures can be also obtained in metallic ones by adequately changing the design parameters,[3,4] for instance in applications as frequency selective surfaces (FSS).

The metallic two-dimensional (2D) photonic lattices studied in this work are designed, built, and simulated for microwave frequencies. These structures are closely related to FSS, which are devices extensively analyzed in the microwave engineering community.[5] FSS are 1D or 2D periodical structures, usually implemented in a single metal layer. Typical applications are filters, bandpass radomes, polarizers, and mirrors. We have used metal cylinders as the basic element in the design of our metallic lattices, constituting a 2D array of metal rods. Several Bravais lattices have been measured and numerically simulated in order to investigate the effects of the symmetry in the band pass edge and higher order photonic band gaps. Two opposite kinds of photonic crystal defects have been investigated: vacancies (elimination of rods from the 2D lattice) and interstitials (extra rods added to the 2D lattice). The first kind of defects introduces allowed frequencies (transmission peaks) inside the photonic band gaps, but also forbidden ones above the band pass edge. Finite interstitial defects are seen to introduce only forbidden frequencies above the frequency band edge.

II. EXPERIMENT

The metal photonic lattice has been fabricated using aluminum calibrated rods having a 5 mm diameter and are 50 cm long, and two supporting Plexiglas plates 0.5×0.5 m^2. In both plates 5 mm diameter holes have been drilled constituting a 36×24 square lattice whose period is 13 mm. These plates allow the design of a large set of metallic lattices: simple square lattices of $13n\times13n$ mm^2 or $13\sqrt{2}n\times13\sqrt{2}n$ mm^2, and simple rectangular lattices of $26n\times13n$ mm^2 ($n=1,2,3,\ldots$), for example. Therefore, the designed structure allows the change of the filling factor within a lattice and the introduction of different kind of defects in each lattice. The photonic 2D lattices are located in the beam path between a transmitter and a receiver 8 element antenna array. The antennas are special designed for broadband applications (1–20 GHz),[6] the integration in eight elements gives an adequate gain in order to focus the microwave beam. The experimental set up is shielded by absorbing pads, reducing reflections by about 40 dB at normal incidence in the range 5–15 GHz, approximately. The antennas are connected through coaxial connectors to a HP-8510C vectorial network analyzer.

III. NUMERICAL SIMULATION

The numerical procedure used for the simulation of the metal photonic lattices materials was the finite difference time domain (FDTD) method.[7] The FDTD directly discretizes the Maxwell curl equations in the time domain, defining a spatial mesh in which the electric and magnetic fields components are located in an alternated fashion.[8] The FDTD technique numerically simulates the time domain evolution of the electromagnetic field in a given region which is numerically described by defining adequate numerical boundary conditions. Because of the periodicity of the structure a single row of the lattice is simulated,[7,9] introducing periodic boundary conditions. Other boundary conditions are

[a]Also at: Institut de Ciencia dels Materials; electronic mail: martinep@uv.es

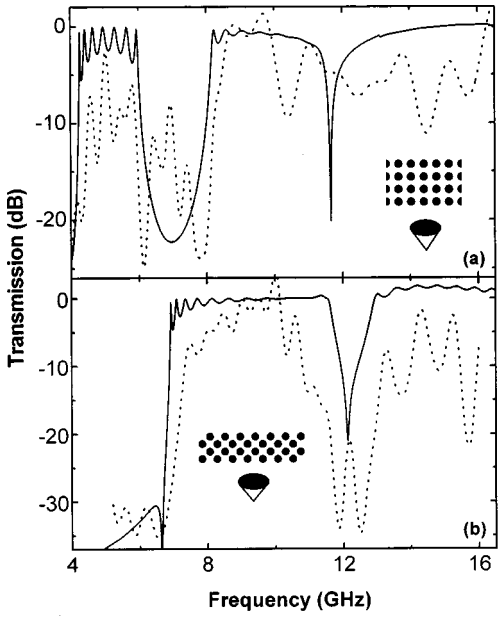

FIG. 1. Experimental (dotted lines) and simulated (continuous lines) transmission spectra for two square photonic lattices: (a) square lattice with 26 $\times 26$ mm^2 unit cell, (b) square lattice observed at 45° with $13\sqrt{2}\times 13\ \sqrt{2}$ mm^2 unit cell. The lattice aspect and observation view is also depicted inside the figure.

zero tangential electric field in the metallic interfaces, and perfect matched layers,[10] the latter are used at the beginning and at the end of the mesh in order to simulate an infinite structure in the x direction at both ends of the mesh. The excitation consisted on a Gaussian shaped wave in the time domain covering the frequency range 0–20 GHz, this is a sine modulated Gaussian in the time domain, its central frequency is the frequency of the sine, and the frequency band is related to the amplitude of the Gaussian envelope. The electric field space distribution is uniform along the y axis, parallel to the y rows of the periodic structures. The frequency response of the photonic crystal has been obtained by a temporal sampling of the transmitted field. Its Fourier transform gives us the transmitted field at each frequency in magnitude and phase. A 2D version of the FDTD is used for an incident transversal electric field parallel to the rods of the 2D lattice. Particularly, we use a nonuniform mesh to model a single x row of the metallic lattice because of its periodicity. Therefore, the FDTD simulations are fast and meaningful because the involved matrices are small, even for complete row defects (analogous to the cases of semiconductor quantum wells and superlattices). Other finite defects should be treated by a full-structure simulation.

IV. RESULTS AND DISCUSSION

Figure 1 presents the obtained transmission spectra in the microwave region of interest for two metallic square 2D lattices. We observe how the FDTD simulated spectra (continuous lines in Fig. 1) reproduces quite well the main features exhibited by the different experimental spectra. The fine structure (resonances in the band pass region) appearing in the simulated results are due to the finite number of rows used in the simulation. A similar modulation is somehow observed in the experimental data because the number of rows used in the different lattices is always below 12, comparable to the 6 or 9 rows simulations.

The characteristic transmittance of a metallic square lattice is first represented in Fig. 1(a), being the dimensions of the unit cell 26×26 mm^2. The expected band pass edge occurs at a frequency $\omega_{g0} = 4.3$ GHz and the width of the first allowed photonic band is 1.7 GHz wide (extracted from the simulated FDTD spectrum). A second photonic band gap extends from $\omega_{g11} = 6$ to $\omega_{g12} = 8.2$ GHz with an extinction ratio around 20 dB. Above ω_{g12} the transmittance turns to be 1 except at 11.7 GHz, where a sharp absorption peak is observed. The experimental frequencies ω_{g0}, ω_{g11}, and ω_{g12} [dotted line in Fig. 1(a)] have approximately the same values as those given earlier from the numerical simulation.

If we reduce a factor $\sqrt{2}$ the dimensions of the square unit cell ($13\sqrt{2}\times 13\sqrt{2}$ mm^2) the filling factor of the corresponding square lattice increases a factor 2. In this case the aspect of the transmittance spectrum is close similar to that shown in Fig. 1(a), but the characteristic frequencies do not shift exactly in the same factor as the lattice constant reduction. Now the band pass edge turns to be $\omega_{g0} = 6.9$ GHz and the second band gap extends from $\omega_{g11} = 8.8$ to $\omega_{g12} = 12.6$ GHz, whereas the width of the first allowed band ($\omega_{g11} - \omega_{g0} = 1.9$ GHz) is practically unchanged. We can also investigate a particular angle of incidence of the electromagnetic wave, namely 45°, whose experimental (dotted line) and simulated (continuous line) transmittance spectra are shown in Fig. 1(b). The value of ω_{g0} becomes unchanged, but the second photonic band gap shifts, narrows ($\omega'_{g11} = 11.5$ and $\omega'_{g12} = 13$ GHz) and changes in shape, being its peak frequency close to ω_{g12} when observed at 0°. Similar values are obtained from the experimental spectrum, which exhibits a broader and deeper second photonic band gap: $\omega'_{g11} = 10.5$ and $\omega'_{g12} = 13.5$ GHz.

A particular example of interest is a rectangular lattice, whose symmetry is lower than the square or hexagonal ones, typically found in the literature. The rectangular unit cell considered here (unit cell 26×13 mm^2) has the same filling factor as the $13\sqrt{2}\times 13\ \sqrt{2}$ mm^2 square unit cell. The difference is introduced by the symmetry, being represented by 180° rotations. If we measure the transmittance normally to the long lattice constant [26 mm, as indicated in the inset of Fig. 2(a)] the shape is closer to a high frequency band pass filter. The experimental transmittance [dotted line in Fig. 2(a)] is practically flat above $w''_{g0} = 6.2$ GHz (6 GHz from the simulation). The FDTD results for the transmission [continuous line in Fig. 2(a)] exhibit two absorbing peaks at 11.6 and 14.7 GHz, the latest having an extinction ratio of about 15 dB, and also a narrow photonic band gap between 16.7 and 18 GHz. The peak at 11.6 GHz correlates with the absorption peak observed at the same frequency in the 26×26 lattice. At the same time, also ω_{g0} agrees with the value of ω_{g11} calculated for that lattice. There are also some coincidences with the characteristic frequencies found in a 13×13 square lattice, whose characteristic frequencies are $\omega_{g0} = 11.85$ GHz (close to the 11.6 GHz peak in the rectangular lattice) and $\omega_{g11} = 14.6$ GHz (close to the 14.7 GHz peak in the rectangular lattice). These particularities arise from the

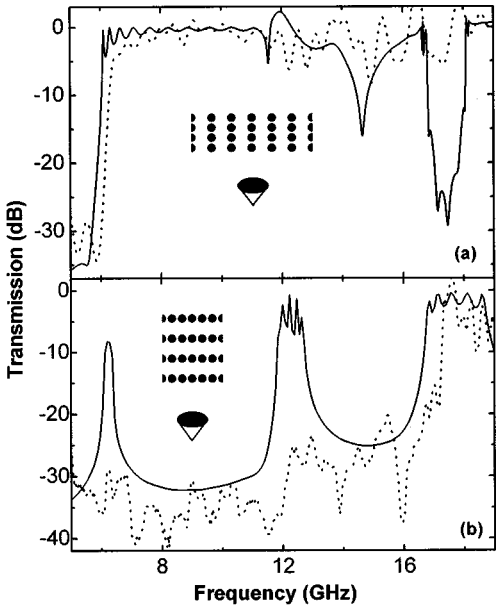

FIG. 2. Experimental (dotted lines) and simulated (continuous lines) transmission spectra for a rectangular lattice with 26×13 mm^2 unit cell observed normally to the long (a) and short (b) lattice distances. The observation view is also depicted inside the figure.

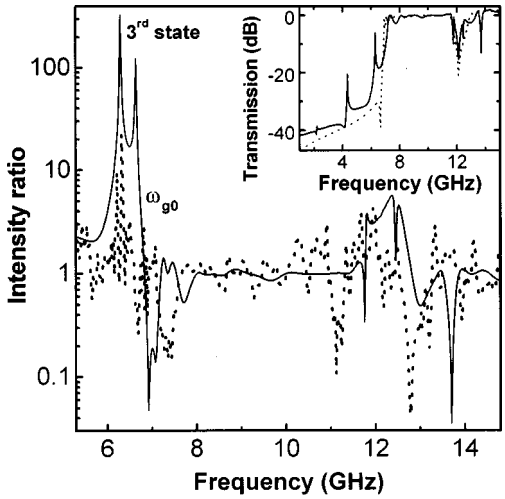

FIG. 3. Calculated (continuous line) and experimental (dotted line) intensity ratios between defect and perfect photonic structures. The perfect lattice is square with a $13\sqrt{2}\times13\sqrt{2}$ mm^2 unit cell. In the defect lattice (quantum-well-like) four complete rows have been removed from the perfect one. The inset shows, for comparison, the simulated transmission spectra for defect (continuous line) and perfect (dotted line) lattices.

coincidence of the equal lattice constants along x and y-axes as those square lattices (26×26 and 13×13 mm^2). Complementary observations can be made when the rectangular lattice is observed normally to the short lattice distance (13 mm), as shown in Fig. 2(b). The simulated transmission spectrum in this case [continuous line in Fig. 2(b)] exhibits a first and narrow transmission peak at 6.2 GHz, instead of the band pass edge shape ($w^{//}_{g0} = 6.2$ GHz) when the lattice was observed normally to the long lattice constant. More important than this first transmission peak (with transmission below 1) is the transmission band beginning at 11.85 GHz, which could be considered as the true $w^{\perp}_{g0}$ (// and $\perp$ stand for direction parallel and perpendicular to the long lattice constant, respectively), because coincides with the value of ω_{g0} given for the square lattice 13×13 mm^2. A second photonic band gap is observed between $w^{\perp}_{g11} = 12.7$ and $w^{\perp}_{g12} = 16.7$ GHz and a third one begins at 18.6 GHz. The experimental spectrum [dotted line in Fig. 2(b)] is not as good as in the precedent cases and only $w^{\perp}_{g12}$ can be clearly determined at 17.3 GHz.

As a conclusion of this first part of our work, we can state that metallic 2D lattices are efficient high frequency pass filters, with added features as the appearance (in the case of square lattices) of high order photonic band gaps. By tuning the lattice symmetry, the lattice distance, and angle of incidence, one can obtain different types of reflecting filters in either narrow or wide frequency bands.

The introduction of defects in these metal lattices enables the possibility for obtaining extremely narrow frequency filters, both for frequency pass and frequency stop, as will be explained later. In equivalent photonic crystals made with dielectric materials, the elimination of dielectric rods from the 2D lattice produces sharp transmission lines (allowed frequencies) inside the photonic band gaps, which are relatively narrow. In metallic photonic lattices the first band gap extends from 0 to ω_{g0} (with absorption ratios stronger than -40 dB) and the allowed frequencies introduced by eliminating metal rods, namely vacancy defects, are well observed in the middle of such a broad photonic band gap. These allowed frequencies are related to transmission peaks with a gain typically below 15 dB (from the absorption background) and a linewidth of about 25 MHz.[11] In the inset of Fig. 3 we compare the simulated transmission spectrum (continuous line) for the $13\sqrt{2}\times13\sqrt{2}$ mm^2 perfect square lattice (12 rows of metallic rods, observed at 45°) and that corresponding to the same structure after removing four complete rows of rods (dotted line). We observe the appearance of several sharp peaks both positive (below the band pass edge) and some negative (above the band pass edge). The three first positive peaks correspond to the three first allowed states for photons inside the first photonic band gap. The fourth allowed state for photons practically coincides with the band pass frequency (a doublet structure centered at 7.35 GHz is obtained from the simulation) of the photonic quantum-well-like structure. The observed shift of the band pass edge in this quantum-well-like structure is due to the finite size of the bulk lattice. It is worth noting that the transmission coefficient is one above the band pass edge in both cases. In the band pass region, three discrete forbidden states are also observed, now like absorption peaks. Two of them appear at frequencies between ω'_{g11} and ω'_{g12} of the perfect lattice, making narrower the second photonic band gap, and the third peak is more intense and appears clearly above ω'_{g12}. Some of these features deduced from our simulation are also observed experimentally, except the first two allowed photonic states below 5 GHz (because of the experimental set up limitations). The best representation to highlight the differences between perfect and defect lattices is the intensity ratio between the measured transmission spectra in both cases, as shown in Fig. 3. The agreement between the

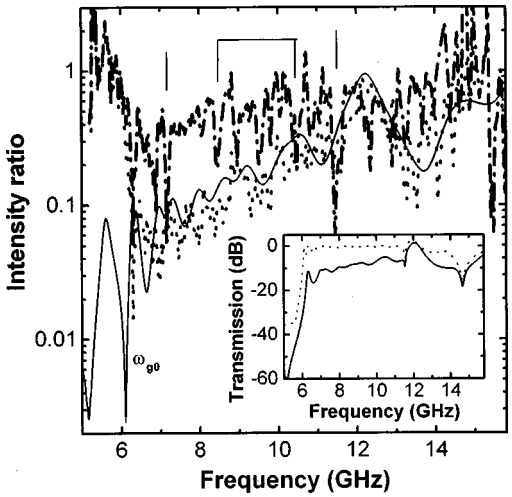

FIG. 4. Experimental intensity ratios for a rectangular lattice with 26×13 mm^2 unit cell in which a row (dotted line) and a 3×3 box (dashed-dotted line) filled with extra rods (new separation along the long lattice distance is 13 mm in the defects). The inset shows, for comparison, the simulated transmission spectra for the one-row filled defect (continuous line) and perfect (dotted line) lattices, whose intensity ratio is shown in the main plot as a continuous line.

ratio obtained from the simulated spectra (continuous line) and that from the experimental ones (dotted line) is reasonably good. Above ω_{g0} the intensity ratio is about one up to the appearance of the high order absorption structures. The third allowed photonic state is observed approximately at the same frequency as the calculated value (6.3 GHz), whereas ω_{g0} and the other high order structures (above 11 GHz) are slightly redshifted.

Finally, we will discuss the case of adding extra rods to a 2D-metal lattice, namely interstitial defects, as first proposed by Sigalas *et al.*[12]. Two kinds of interstitial defects inside a rectangular lattice [that presented in Fig. 2(a)] have been measured: (1) an extra filled row (rods separated 13 mm) and (2) a 3×3 box of extra rods (box with a square unit cell 13×13 mm^2). Their corresponding intensity ratio with respect to the perfect lattice has been represented in Fig. 4. The frequency dependence of the intensity ratio in both cases are clearly different from that found for vacancy defects (Fig. 3). For the periodical one-row-interstitial defect (dotted and continuous lines—experimental and numerical—in Fig. 4), case (1), the main feature is the absence of peaks either positive or negative and an intensity ratio that remains always below 1. If a 1D lattice with rods separated by 13 mm was considered the transmitted field would be a monotonically increasing function without any cut-off frequency.[13] Therefore, the behavior exhibited by the inserted row inside the rectangular lattice can be explained by the convolution of the transmitted field for both perfect lattices, the 1D and the 2D ones. The intensity ratio from simulated spectra (see the inset of Fig. 4 for the comparison of the transmission spectra) nicely accounts for the smooth variations of the measured intensity ratio with frequency. Our FDTD method cannot be used in a simple way for nonperiodical defects embedded in the lattice and any simulation is presented for case (2). In this structure we observe how the intensity ratio (dashed-dotted line in Fig. 4) is now nearer to one and extremely narrow absorption peaks (some of them are indicated by short lines in Fig. 4) appears above $w^{//}_{g0}$. The fact that the defect is spatially finite (as compared to the dimensions of the crystal) prevents for excessive losses as occurs in case (1). On the other hand, the geometry of the defect will produce a zero dimensional confinement for photons (quantum-box-like defect), giving rise to the observed discrete absorption peaks.

V. CONCLUSIONS

Several metal rod based photonic structures with different symmetry have been experimentally studied. In all cases (with and without defects) the experiment is well accounted for by using a numerical 2D-FDTD technique. We have shown the influence of design parameters (symmetry of the lattice, filling factor, and kind of defects) on the transmitted electromagnetic field. The main characteristic effect of introducing vacancy defects in the photonic lattices is the appearance of allowed frequencies in the first photonic band gap. In the case of interstitial rods added to a photonic lattice, only spatially finite defects (quantum-box-like) introduce discrete forbidden frequencies above the band pass edge frequency.

ACKNOWLEDGMENT

This research has been supported by the Universitat de València, project UV 98-2719.

[1] J. D. Joannopoulos, P. R. Villeneuve, and S. Fan, Nature (London) **386**, 143 (1997).
[2] S. Gupta, G. Tuttle, M. Sigalas, and K-M. Ho, Appl. Phys. Lett. **71**, 2412 (1997).
[3] R. E. Collin, *Field Theory of Guided Waves* (IEEE Press, New York, 1991).
[4] E. Brown and O. B. McMahon, Appl. Phys. Lett. **67**, 2138 (1995).
[5] *Frequency Selective Surfaces and Grid Arrays*, edited by T. K. Wu (Wiley, New York, 1995).
[6] C. Reig, E. A. Navarro, and V. Such, IEEE Trans. Antennas Propag. **45**, 1484 (1997).
[7] E. A. Navarro, B. Gimeno, and J. L. Cruz, Electron. Lett. **29**, 446 (1993).
[8] E. A. Navarro, N. T. Sangary, and J. Litva, IEEE Trans. Microwave Theory Tech. **44**, 1115 (1996).
[9] J. A. Roden, S. D. Gedney, M. P. Kesler, J. G. Maloney, and P. H. Harms, IEEE Trans. Microwave Theory Tech. **46**, 420 (1998).
[10] J. P. Berenger, J. Comput. Phys. **114**, 185 (1994).
[11] D. R. Smith, S. Schultz, N. Kroll, M. Sigalas, K. M. Ho, and C. M. Soukoulis, Appl. Phys. Lett. **65**, 645 (1994).
[12] M. M. Sigalas, C. T. Chan, K. M. Ho, and C. M. Soukoulis, Phys. Rev. B **52**, 11744 (1995).
[13] J. Carbonell, O. Vanbésien, and D. Lippens, Superlattices Microstruct. **22**, 597 (1997).